Drop Impingement onto a Wetted Surface: Effects of Gravity and Shape

Murat Dinc and Donald D. Gray

***Abstract*—** Single water drops impinging onto wet, flat, isothermal surfaces have been simulated numerically to investigate the influence of gravity level and drop shape on the resulting flow. The commercial code ANSYS 14 Fluent was employed to perform 2D-axisymmetric simulations for incompressible, laminar and unsteady flow conditions using the explicit Volume of Fluid (VOF) surface tracking method with the Piecewise Linear Interface Calculation scheme (PLIC), the Continuum Surface Force model (CSF), and adaptive mesh refinement. Simulations of a spherical water drop impacting an upward facing wet surface (Re = 6690, We = 139, h/D = 0.837, θ = 0°) were performed for different gravity conditions based on some of the planets and asteroids in our Solar System. These are Solar surface gravity (g = 275 m/s^2), Jupiter surface gravity (g = 24.8 m/s^2), Earth surface gravity (g = 9.81 m/s^2), Mars surface gravity (g = 3.7 m/s^2), Lunar surface gravity (g = 1.68 m/s^2), Pluto surface gravity (g = 0.61 m/s^2), asteroid Vesta surface gravity (g = 0.252 m/s^2), asteroid 1999RQ-36 surface gravity (g = 0.038 m/s^2), and zero gravity (g = 0). While the general evolution of the craters was similar, the rate at which they evolved increased as the value of g increased. The impact of an upward moving drop on a downward facing layer in Earth surface gravity (g = –9.81 m/s^2) caused a significantly different flow. Because laboratory observations have found that water drops in the size range under study deviate slightly from true spheres, three cylindrical drops, one having same diameter and mass as a spherical drop and the others having same diameters but different masses, were simulated. The flows produced by the cylindrical drops were sufficiently similar to that produced by a sphere of equal volume that it will not be necessary to account for the much smaller deviations from sphericity which occur in reality in order to obtain realistic simulations.

***Keywords*—**CFD, Fluent, VOF, drop, gravity, impact dynamics.

I. Introduction

The interaction of drops and sprays with wet and dry surfaces is the key feature in many engineering applications such as spray cooling, spray painting, and fuel injection systems [1]. A first-principles simulation of a spray of millions of drops is impractical using present computers. The goal of this project is to develop correlations for inclusion in a Monte Carlo spray cooling model [2] which will embody sufficient physics to yield reliable predictions while being computationally efficient enough to use as a practical design tool. This paper reports one step in a study of the spray cooling of heated surfaces by presenting computer simulations of single water drops which are spheres or cylinders of diameter D moving at velocity U normal to initially motionless thin layers of water having thickness h. The water has density ρ and dynamic viscosity μ, and surface tension coefficient σ. The ambient fluid was air at sea level pressure (101.3 kPa absolute). All fluids were at 15°C.

The impact of liquid drops onto both dry and wet surfaces has been studied by many researchers for more than a century [3]. The interaction between a drop and a surface may involve inertial, viscous, surface tension, and gravitational forces. A sufficient set of dimensionless numbers to describe the interaction of these forces is the Reynolds number ($Re = \rho UD/\mu$), the Weber number ($We = \rho U^2 D/\sigma$), and the Froude number ($Fr = U^2/gD$, where g is the acceleration due to gravity). The Reynolds number is proportional to the ratio of inertial forces to viscous forces, the Weber number is proportional to the ratio of inertial to surface tension forces, and the Froude number is proportional to the ratio of inertial to gravity forces. Another key dimensionless number is the relative layer thickness (h/D).

Fig. 1 shows the typical flow when a drop with an initial diameter (D) and initial velocity (U) impacts onto a wet surface as obtained from a 2D-axisymmetric simulation. The impact drives the liquid outward from the point of impact forming a crater whose leading edge takes the form of a crown. This may be accompanied by the ejection of droplets known as prompt splashing [3]. The crown grows as in height as it spreads until it reaches a maximum crown height (H_{max}) at time t_{max}. The crown may become unstable to the formation of jets which in turn may pinch off to form droplets (late splashing), although this is an inherently three dimensional phenomenon that cannot be captured by the axisymmetric simulations reported here. In the final stage the crown collapses and the crater refills, with the possible formation of a Worthington jet at the center due to the converging inflow.

This paper is focused on the effects of gravity and drop shape. Future spacecraft, satellites, and landers may incorporate electronic packages that will require advanced spray cooling systems that can operate in a wide range of gravity fields. This is the motivation for studying the effects of a range of g values in this paper.

Murat Dinc is with West Virginia University, Morgantown, WV 26506-6103 USA (phone: 775-200-6620; e-mail: mdinc@mix.wvu.edu).

Donald D. Gray is with West Virginia University, Morgantown, WV 26506-6103 USA (e-mail: Donald.Gray@mail.wvu.edu).

The authors gratefully acknowledge the financial support of this work under NASA Cooperative Agreement NNX10AN0YA. The views and conclusions are those of the authors and should not be interpreted as necessarily representing the official policies or endorsements of NASA or the West Virginia NASA Space Grant Consortium.

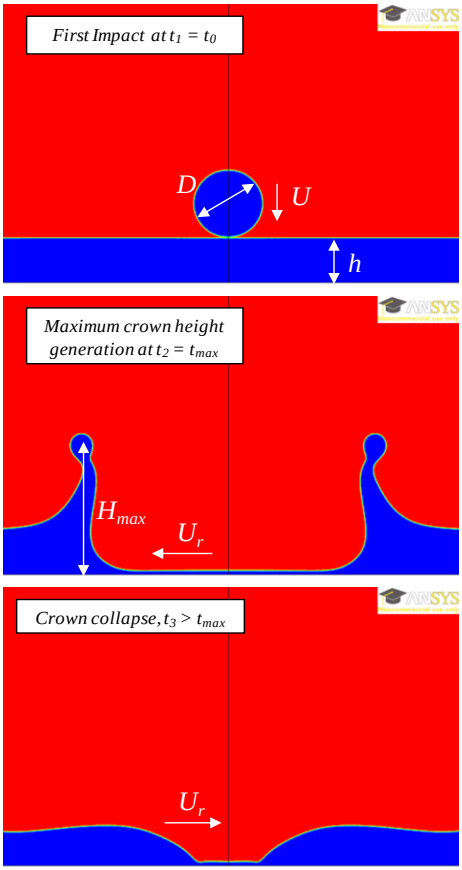

Fig. 1 Typical single drop impact on a wet, flat surface: first impact at $t_1 = t_0$ (top image), maximum crown height at $t_2 = t_{max}$ (middle image) and crown collapse as liquid refills crater at $t_3 > t_{max}$ (bottom image)

High speed videos obtained in the experimental phase of this research project have shown that water drops in the size range under study (D > 4 mm) deviate slightly from true spheres as they fall (Fig. 2). This observation is the motivation for simulating the effects of non-spherical drop shapes in this paper.

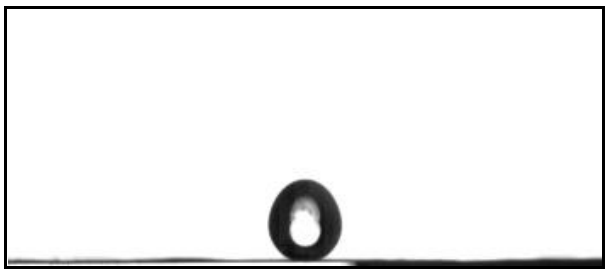

Fig. 2 Shape of initially spherical water drop right before impact onto water layer for *We* = 663, *Re* = 17 100, *Fr* = 113 [4]

II. Computational Method

Computational Fluid Dynamics (CFD) has matured into an indispensable tool in many areas of science and engineering including multiphase flow applications such as sprays and drops. Ariafar [5] modeled turbulent supersonic flow in a thermocompressor using the commercial CFD code Fluent. Ghandriz and Goudarzi [6] used the Volume of Fluid (VOF) model for simulating two-phase flow in a container with a moving floor. Shao et al. [7] used Fluent to simulate the complex flow field in a quenching furnace with a spray of nitrogen gas and water. Heat and mass transfer from a single drop in a saturated solvent vapor environment was simulated using the finite volume method by Torfi and Nejad [8].

The computational simulations reported here were obtained using the commercial CFD code ANSYS 14 Fluent on a desktop workstation. The Navier-Stokes and continuity equations were solved in 2D-axisymmetric coordinates using the finite volume method for unsteady, incompressible, laminar flow. In this flow, it is essential to be able to determine the location of the free surface of the liquid. This was accomplished by using the explicit Volume of Fluid (VOF) method [9]. The VOF multiphase model was implemented such that the drop liquid and the layer liquid could be distinguished, even though they are physically identical. For each liquid an advective transport equation was solved for an indicator function defined as the fraction of a computational grid cell occupied by that liquid. If the sum of these liquid indicator functions was less than 1, the cell contained an air-water interface at which surface tension acted. Each fluid was treated as incompressible, and volume weighted fluid properties were used in cells which contained air and water. Surface tension was incorporated into the Navier-Stokes equation by using the Continuum Surface Force (CSF) model, which accounts for the curvature of the interface [10].

Velocity and pressure coupling was achieved with the Pressure Implicit with Splitting of Operators (PISO) algorithm [11]. The sharpness of the interface was enhanced by use of the geo-reconstruct (Piecewise Linear Interface Calculation, PLIC) scheme [12]. Discretization of the advective terms in the momentum equations used second order upwinding. Solution convergence was assured by monitoring the mass imbalance at some points in the domain and also by checking the residual values of parameters such as the velocity far from the impact region.

The initial drop diameter D, the liquid layer thickness h, and the drop velocity U were defined as initial conditions. The boundary conditions are shown in Fig. 3 with a grid that shows the initial mesh. The impermeable no-slip wall boundary condition was applied on the bottom boundary, and the centerline was a symmetry boundary. Pressure outlet boundary conditions were defined on the top and maximum radius boundaries.

A great improvement in computational speed was achieved without sacrificing solution accuracy by using the adaptive mesh refinement method in which the grid was automatically refined in critical areas of rapid change such as the liquid-gas interface, and coarsened in areas of little change. In each level of refinement, the mesh length (both in vertical and horizontal directions) was divided by 2. For the present domain, a uniform grid of square D/80 cells would contain 325 000 cells. By using adaptive mesh refinement with the largest cells measuring D/5 and the smallest cells measuring D/80, only 25 000 cells were needed.

For validation purposes some simulations were compared to computational and experimental studies in the literature, and

they were found to be in good agreement. As an example, Fig. 4 shows a comparison with the physical experiment of [13] and the computational study of [14].

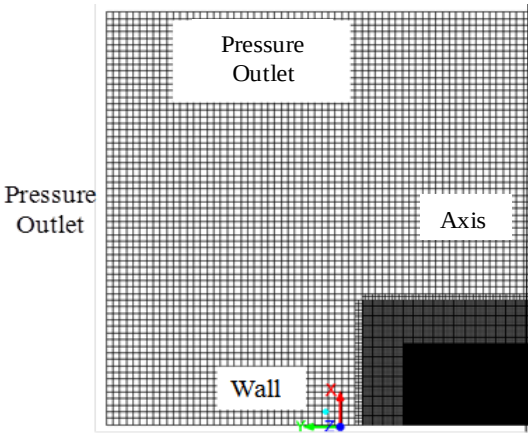

Fig. 3 Boundary conditions and initial mesh for 2D-axisymmetric computational domain (0.05 m x 0.05 m)

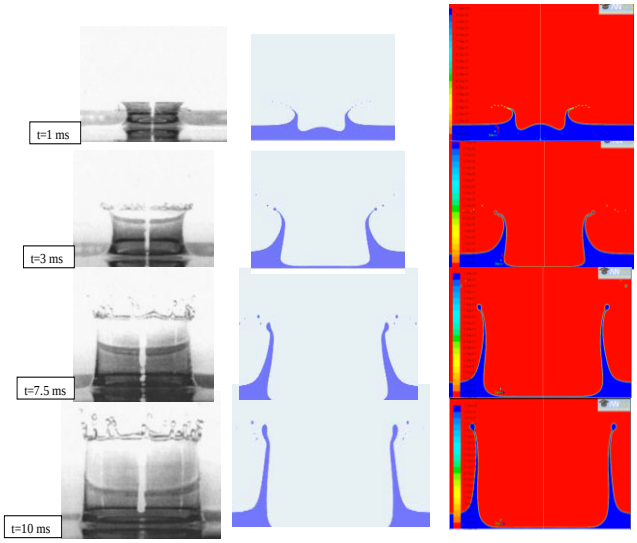

Fig. 4 Comparison of results for 4.2 mm diameter droplet impacting onto a liquid layer with a thickness of 2.1 mm: *Re = 1168*, *We* = 2009, *Fr* = 631, and *h/D* = 0.5. *(Experimental images from* [13] *in the left column, numerical results from* [14] *in the middle column, and numerical results of the current study in the right column with blue representing water and red representing air.)*

Fig. 5 shows the comparison of another simulation with an experiment performed by our experimentalist collaborators [4]. Very good agreement with the experimental results was obtained based on the free surface shape and flow dynamics.

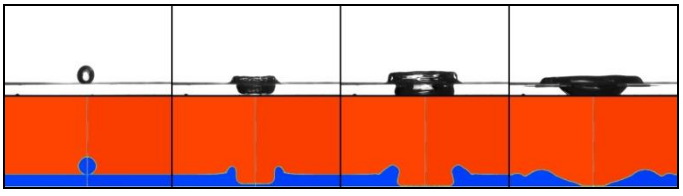

Fig. 5 Comparison of the high-speed video images (top) and the CFD simulations (bottom) for times $t \approx 0$, 3.67, 8.92, and 17.8 ms (*We* =166, *Re* = 6370, *Fr* = 136, *h/D* = 0.666) [4]

III. Results

A. General Results

Since the aim of this study was the investigation of gravity and drop shape for a single water drop impingement onto a water layer, only the magnitude of *g* was varied. For all of these cases *D* = 4.48 mm, *h* = 3.75 mm, and *U* = 1.5 m/s. Therefore, *We*, *Re*, and *h/D* were the same for all simulations performed, whereas *Fr* varied. In all cases, the general sequence of events is that the drop impact creates a growing crater surrounded by an elevated crown. The crater contains a very thin liquid layer with thickness equal to about 2% of the drop diameter. The crater reaches a maximum radius, begins to refill, and the inrushing liquid creates an incipient Worthington jet (except in the negative Earth gravity case). No splashing was predicted. In the next sections, the effects of gravity and drop shape will be presented in detail.

B. Effects of Gravity

Simulations were performed for eight upward facing layers with *g* ranging from that of the Sun (275 m/s^2) to that of the 500 m-diameter asteroid 1999RQ-36 (0.038 m/s^2). Solar gravity is an upper bound for applications in this stellar system and dramatizes the effects of very high *g* values. Asteroid 1999RQ-36 is of interest because it approaches Earth every six years and is a likely target for a sample return mission [15]. Case 9 was for zero gravity, and Case 10 was for an upward moving drop hitting a downward facing layer in Earth gravity.

Table I displays the values of *g* and the dimensionless parameters for these simulations. It is seen that *Fr* was the only dimensionless number which varied. In all these cases, the contact angle was set to 0°, which had no effect on the results because for this contact angle the wall is always wet.

Table I Parameters used in gravity simulations

Case	Name	Gravity (m/s^2)	*Re*	*We*	*Fr*	*h/D*
1	Sun	275	6690	139	1.83	0.837
2	Jupiter	24.8	6690	139	20	0.837
3	Earth	9.81	6690	139	51	0.837
4	Mars	3.7	6690	139	136	0.837
5	Moon	1.68	6690	139	310	0.837
6	dwarf planet Pluto	0.61	6690	139	823	0.837
7	asteroid Vesta	0.252	6690	139	1990	0.837
8	asteroid 1999RQ-36	0.038	6690	139	13 200	0.837
9	zero gravity	0	6690	139	∞	0.837
10	"negative" Earth gravity	-9.81	6690	139	-51	0.837

Fig. 6 shows that the dimensionless time (*tU/D*) at which liquid started to refill the crater increased as *Fr* increased, showing that gravity as well as surface tension caused the

craters to refill. It is curious that the results approximately follow a straight line until Pluto on this semi-log plot. The dimensional times were 9, 26, 34, 42, 45, 49, 49, 51 ms for Cases 1-8, respectively. Fig. 7 shows that the dimensionless times at which the Worthington jet reached the initial undisturbed layer thickness also increased with *Fr*. In this plot the approximate linear trend continues until Vesta. The pace of events increased as *Fr* increased (Fig. 7).

Fig. 8 shows the centerline liquid layer thickness, h_0, as a function of time for Solar, Jupiter and Earth gravity. Fig. 9 shows similar results for Earth, Mars and Vesta gravity in order to see the effects of lower gravity compared to Earth. The initial decrease in centerline thickness and the minimum thickness are only slightly affected by gravity. In contrast, the maximum height of the Worthington jet is greatly increased by increasing gravity, while the time of maximum height is greatly reduced. In general, the time scales of the flow are faster when the gravity is higher. Figures 10 through 18 show the configuration of the liquid during the impact process for Cases 1-9 respectively. The trends of faster, more extreme deformations with increasing gravity are confirmed by these results. Of course, in the case of zero gravity (Case 9), the refilling of the crater was accomplished through surface tension alone. The zero gravity simulation was discontinued before the formation of a Worthington jet could occur. The faster rate of evolution produced by higher *g* is illustrated by the well-defined Worthington jet at 13 ms in Solar gravity (Fig. 10) whereas the jet has barely begun to form at 45 ms in Mars gravity (Fig. 13). It should be noted that splashing was not observed in Cases 1-9 as shown in Figs. 10 to 18.

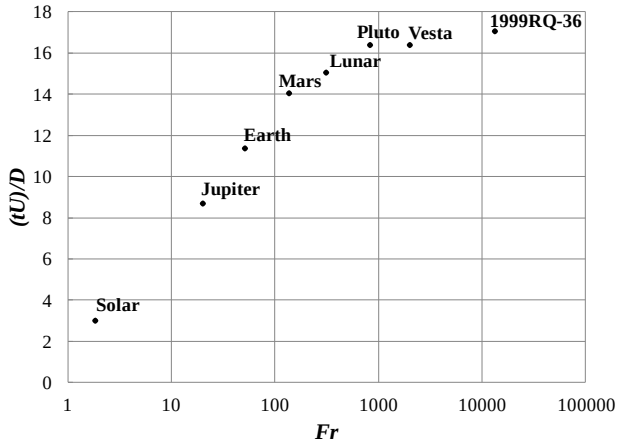

Fig. 6 The effect of *Fr* on the time at which the crater started to refill

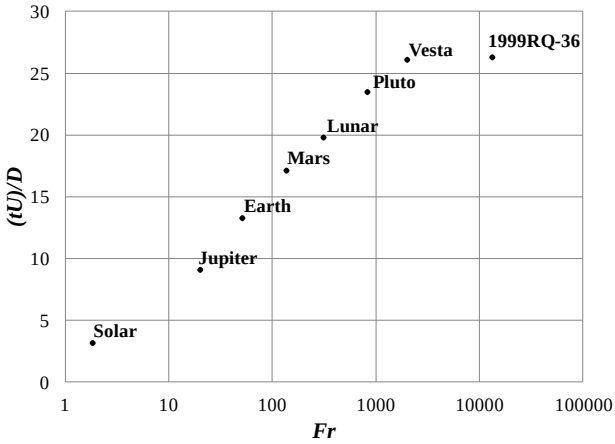

Fig. 7 The effect of *Fr* on the time at which the Worthington jet reached the undisturbed layer thickness

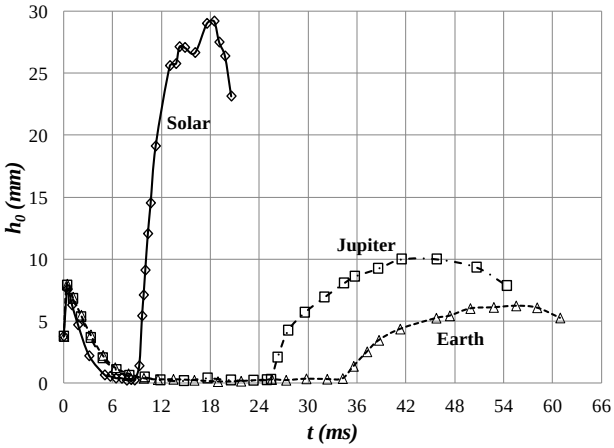

Fig. 8 Centerline liquid layer thickness, h_0, as a function of time for Solar, Jupiter and Earth gravity

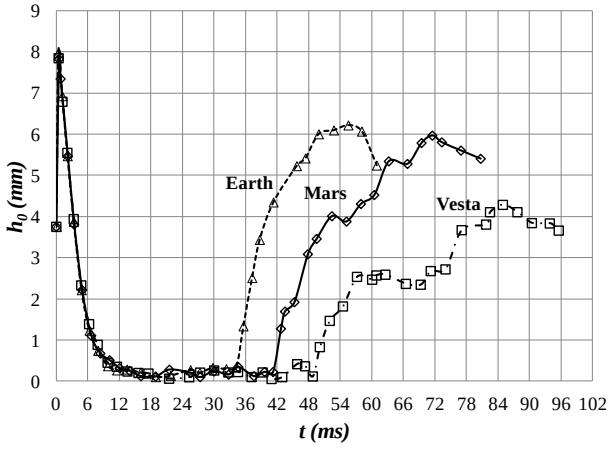

Fig. 9 Centerline liquid layer thickness, h_0, as a function of time for Earth, Mars and Vesta gravity

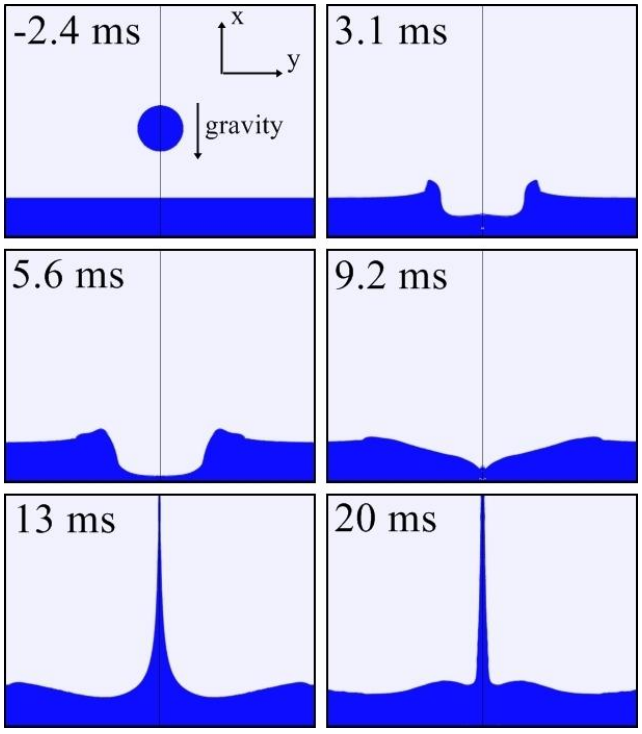

Fig. 10 Case 1: single drop impact onto a wet surface in Solar gravity *(Note: blue is water and white is air. "ms" refers to milliseconds. Each image are cropped in order to zoom in on the impact and crater region)*

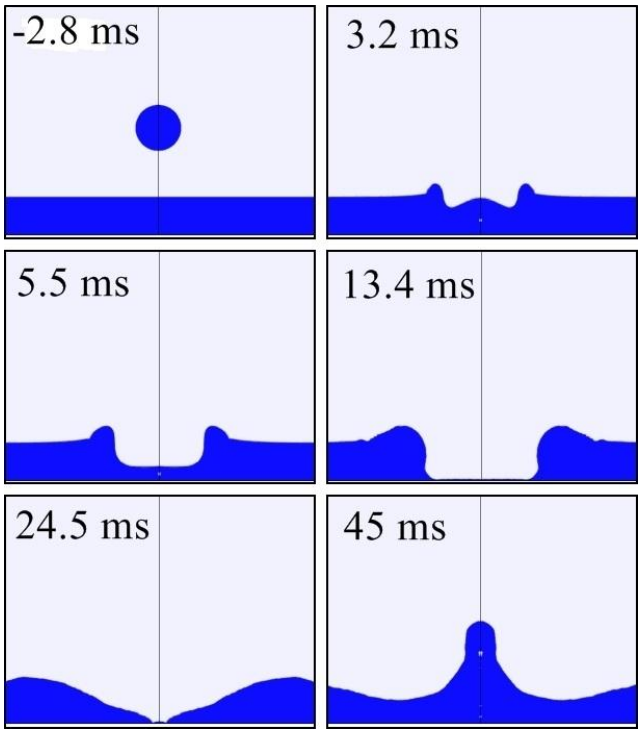

Fig. 11 Case 2: single drop impact onto a wet surface in Jupiter gravity *(Note: blue is water and white is air. "ms" refers to milliseconds)*

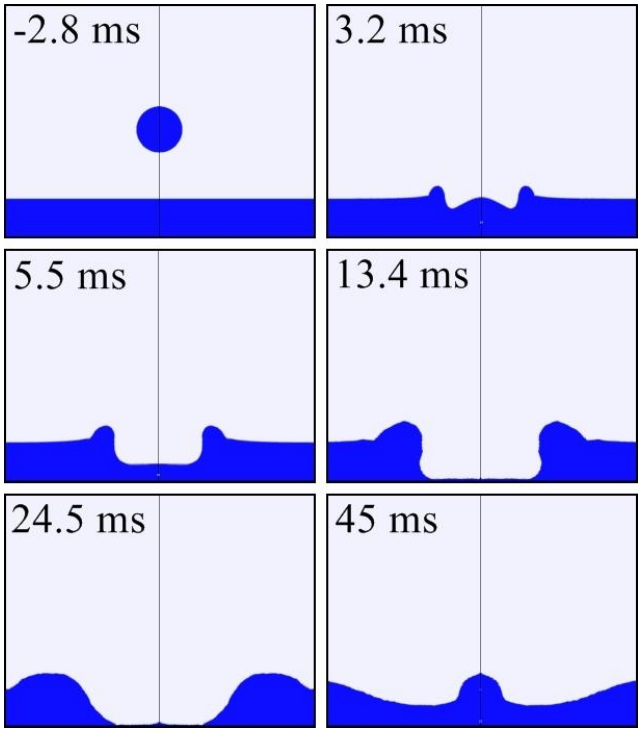

Fig. 12 Case 3: single drop impact onto a wet surface in Earth gravity *(Note: blue is water and white is air. "ms" refers to milliseconds)*

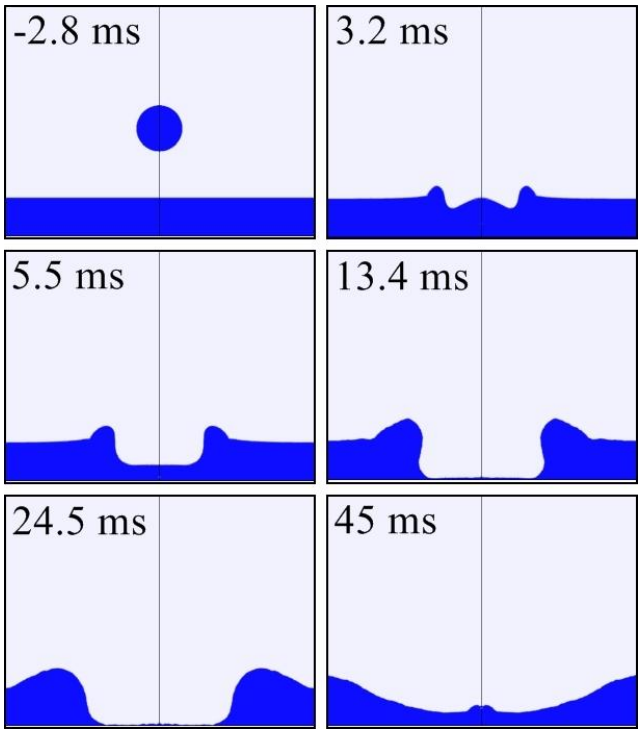

Fig. 13 Case 4: single drop impact onto a wet surface in Mars gravity *(Note: blue is water and white is air. "ms" refers to milliseconds)*

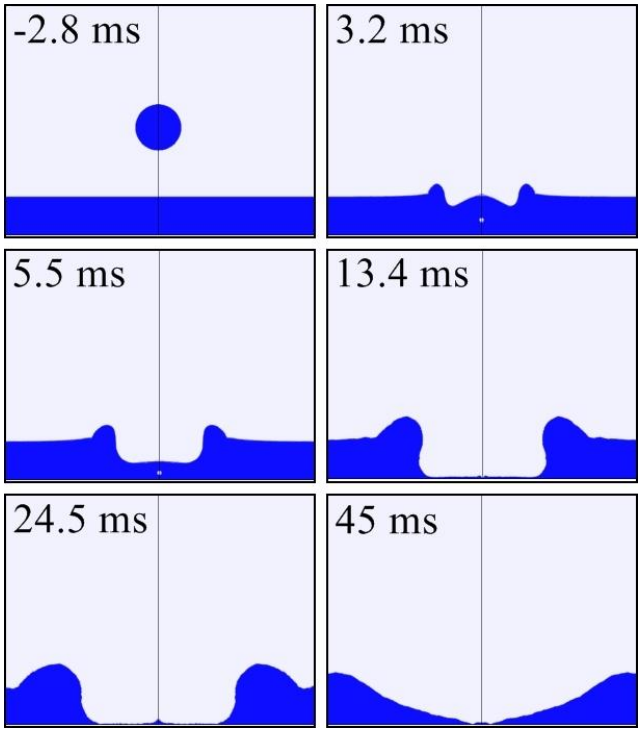

Fig. 14 Case 5: single drop impact onto a wet surface in Lunar gravity *(Note: blue is water and white is air. "ms" refers to milliseconds)*

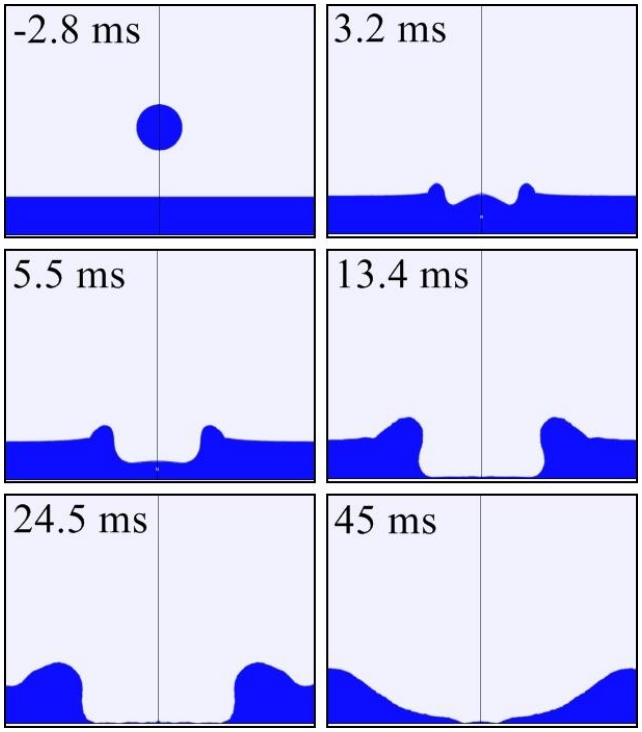

Fig. 16 Case 7: single drop impact onto a wet surface in asteroid Vesta gravity *(Note: blue is water and white is air. "ms" refers to milliseconds)*

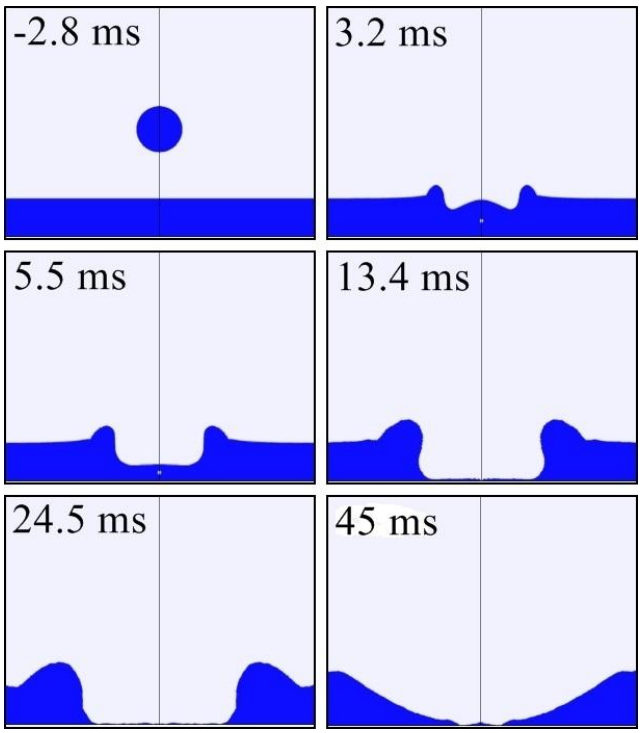

Fig. 15 Case 6: single drop impact onto a wet surface in Pluto gravity *(Note: blue is water and white is air. "ms" refers to milliseconds)*

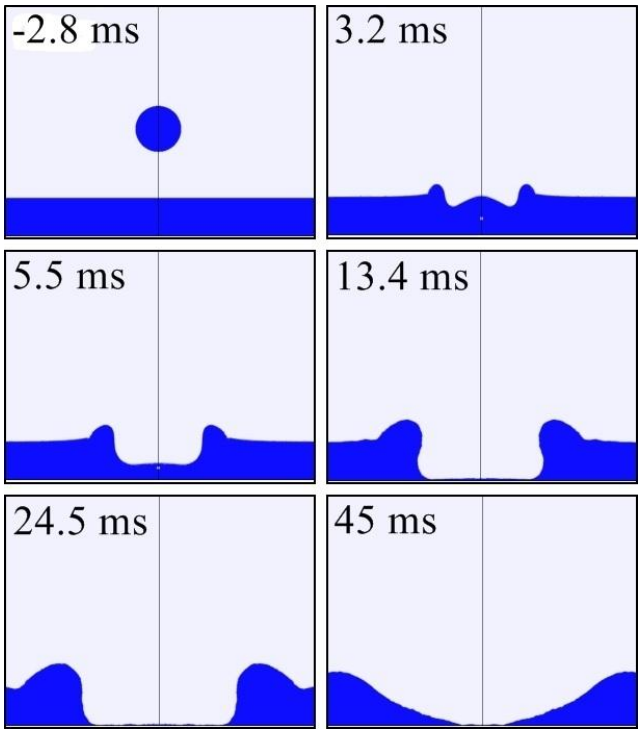

Fig. 17 Case 8: single drop impact onto a wet surface in asteroid 1999RQ-36 gravity *(Note: blue is water and white is air. "ms" refers to milliseconds)*

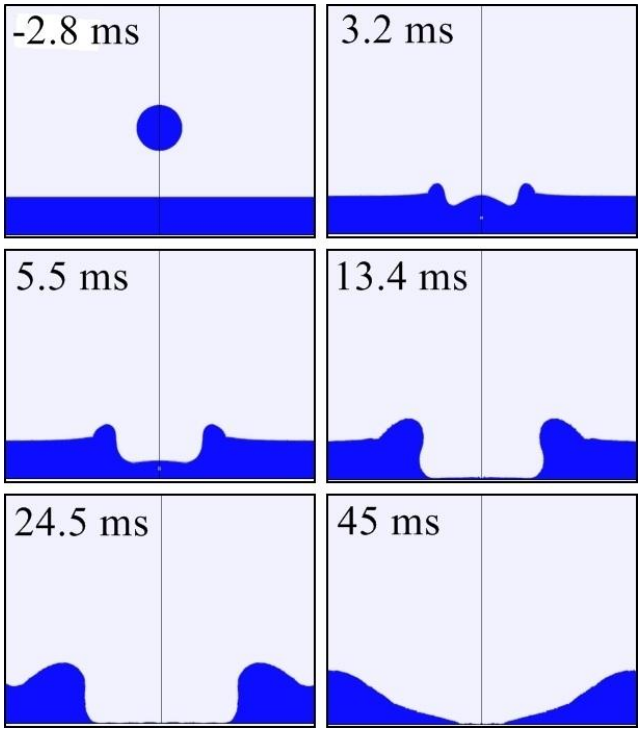

Fig. 18 Case 9: single drop impact onto a wet surface in zero gravity *(Note: blue is water and white is air. "ms" refers to milliseconds)*

The "negative gravity" flow of an upward moving drop hitting a downward facing liquid layer in Earth surface gravity (Case 10, $Fr = -51$) is shown in Fig. 19. There was still no splashing, but the impact excited a Rayleigh-Taylor instability in which the crown of the impact crater grew large as it fell away from the surface. The crater continued to spread until most of the liquid fell from the surface (Fig. 20).

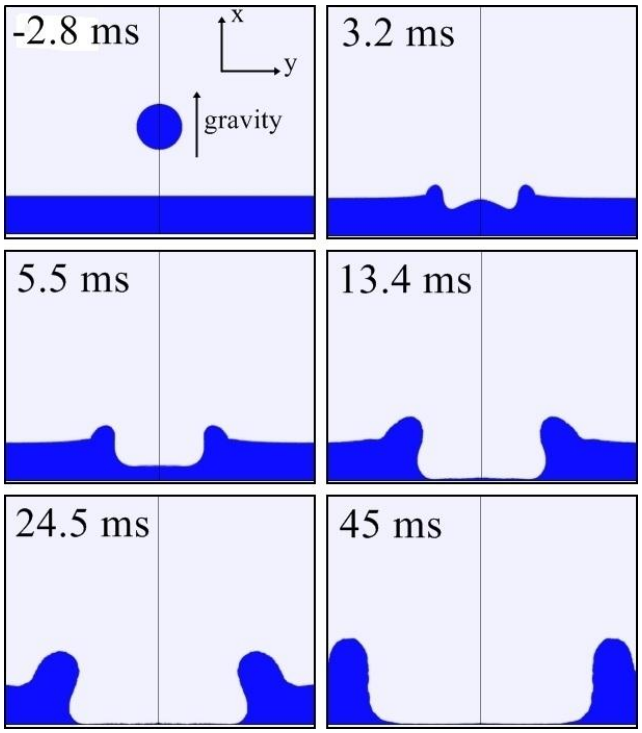

Fig. 19 Case 10: single drop impact onto a wet surface in "negative Earth gravity". The ceiling is at the bottom of this figure.

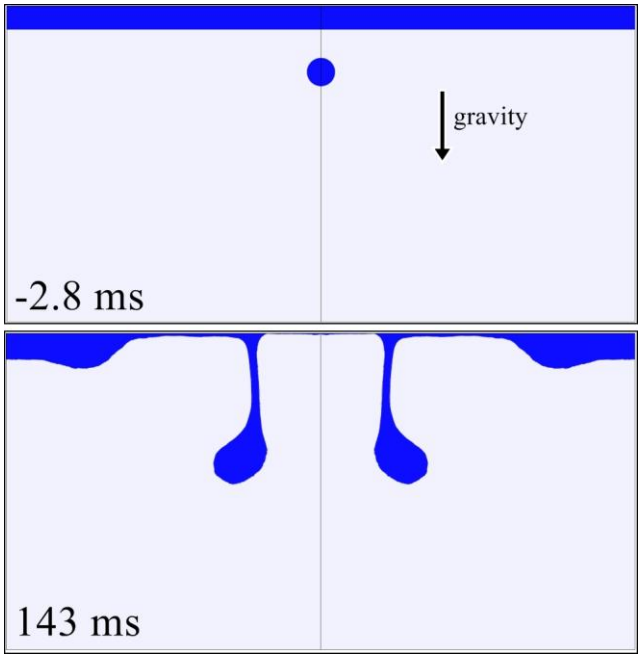

Fig. 20 Case 10: liquid crown falling off the surface for upward moving drop hitting the downward facing water layer in Earth gravity ("Negative Earth Gravity"). The ceiling is at the top of this figure. *(Note: original domain size is shown)*

C. *Effects of Drop Shape*

High speed videos obtained in the experimental phase of this research project demonstrated that drops in the 4-mm size range are seldom truly spherical [4]. Instead they quiver about a spherical mean. In order to determine if deviations from sphericity would have a significant effect on the drop impact flow, computations were performed for cylindrical "drops" which represent a more extreme deviation from a spherical shape than is ever observed in the laboratory. Simulations were performed for single cylinders of water with a diameter D = 4.48 mm (the same as for the previously described spherical drops) and altitudes L of 4.48, 2.99 and 2.24 mm impinging onto static water layers with thickness h = 3.75 mm in Earth gravity. These altitudes were chosen to create cylinders of equal height, equal volume (and mass), and half height, respectively, compared to the Case 3 reference sphere. Table II shows the parameters for these cases, where D is the length scale used to calculate Re, We, and Fr. A contact angle of 0° was specified in all these cases, but did not affect the results.

Table II Parameters used to study drop shape

Shape	***Re***	***We***	***Fr***	***h/D***	***L/D***
Case 3 sphere	6690	139	51	0.837	NA
Equal altitude cylinder	6690	139	51	0.837	1
Equal volume cylinder	6690	139	51	0.837	0.667
Half altitude cylinder	6690	139	51	0.837	0.5

Results for the Case 3 sphere and the cylindrical drops have been presented in Figs. 21-25 and in Tables III and IV. Figure 21 shows that the crater shapes are nearly identical for the Case 3 spherical drop and the equal volume cylinder, which has altitude $L = 2D/3$. The only noticeable difference between the two is that the small air bubble trapped by the flat underside of the cylinder at 3.2 ms is larger than the bubble trapped by the sphere. The more prominent bubble formation under the cylinder may be attributed to the greater difficulty for the air to flow out from beneath the flat bottom of the cylinder. Figure 22 shows that there is very little quantitative difference in the time history of the layer thickness on the impact axis, thus confirming the visual impression given by Figure 21. Further confirmation is provided by Table III which shows the dimensionless time at which the impact crater started to refill, and Table IV which shows the dimensionless time at which the Worthington jet reached the initial undisturbed free surface thickness. For both times, the difference between the sphere and the equal volume cylinder is less than 0.5%. These comparisons suggest that the much less severe deviations from perfect sphericity which actually occur will have insignificant effects on the flows, at least at these values of dimensionless numbers.

The equal altitude and half altitude cylinder impacts are shown in Figs. 23 and 24, respectively. As the volume of the cylindrical drop increases, the crater spreads to a greater radius, the crown reaches a greater height, and the Worthington jet becomes more prominent. At 45 ms, the Worthington jet was thinnest for the equal altitude cylinder and fattest for the half altitude cylinder while it was very similar to the spherical drop for the equal volume cylinder. The trapped air forms a ring bubble for the half altitude cylinder as seen in Figs. 24 and 25 (b) while a single "spherical" bubble is formed under the full altitude cylinder as shown by Figs. 23 and 25 (a). In the case of the half altitude cylinder, a secondary drop is also observed on the centerline at 14.2 ms. Tables III and IV show that the dimensionless time at which the crater begins to refill and the dimensionless time the Worthington jet reaches the elevation of the undisturbed free surface both increase with increasing cylinder volume. Because the differences in shape between a sphere and a cylinder are far more extreme than the differences observed among actual drops in the lab, it can be concluded that it is not necessary to simulate realistic nonspherical drops. Simulations of spherical drops are sufficiently accurate.

Table III The effect of drop shape on the time at which the crater started to refill

Shape	***Drop Volume Ratio*** ($V_{cylinder}/V_{sphere}$)	***L/D***	***(tU)/D***
Case 3 sphere	NA	NA	11.40
Equal altitude cylinder	1.5	1	12.77
Equal volume cylinder	1	0.667	11.45
Half altitude cylinder	0.75	0.5	9.76

Table IV The effect of drop shape on the time at which the Worthington jet reached the undisturbed layer thickness

Shape	***Drop Volume Ratio*** ($V_{cylinder}/V_{sphere}$)	***L/D***	***(tU)/D***
Case 3 sphere	NA	NA	13.29
Equal altitude cylinder	1.5	1	13.61
Equal volume cylinder	1	0.666	13.27
Half altitude cylinder	0.75	0.5	11.83

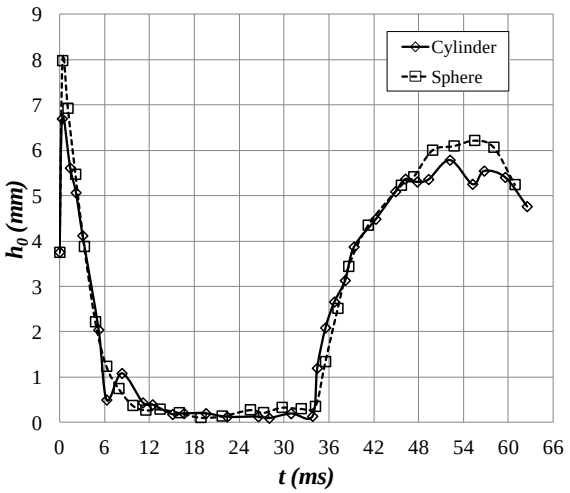

Fig. 21 Variation of the centerline liquid layer thickness, h_0, with time for the Case 3 sphere and the cylindrical drop having the same volume

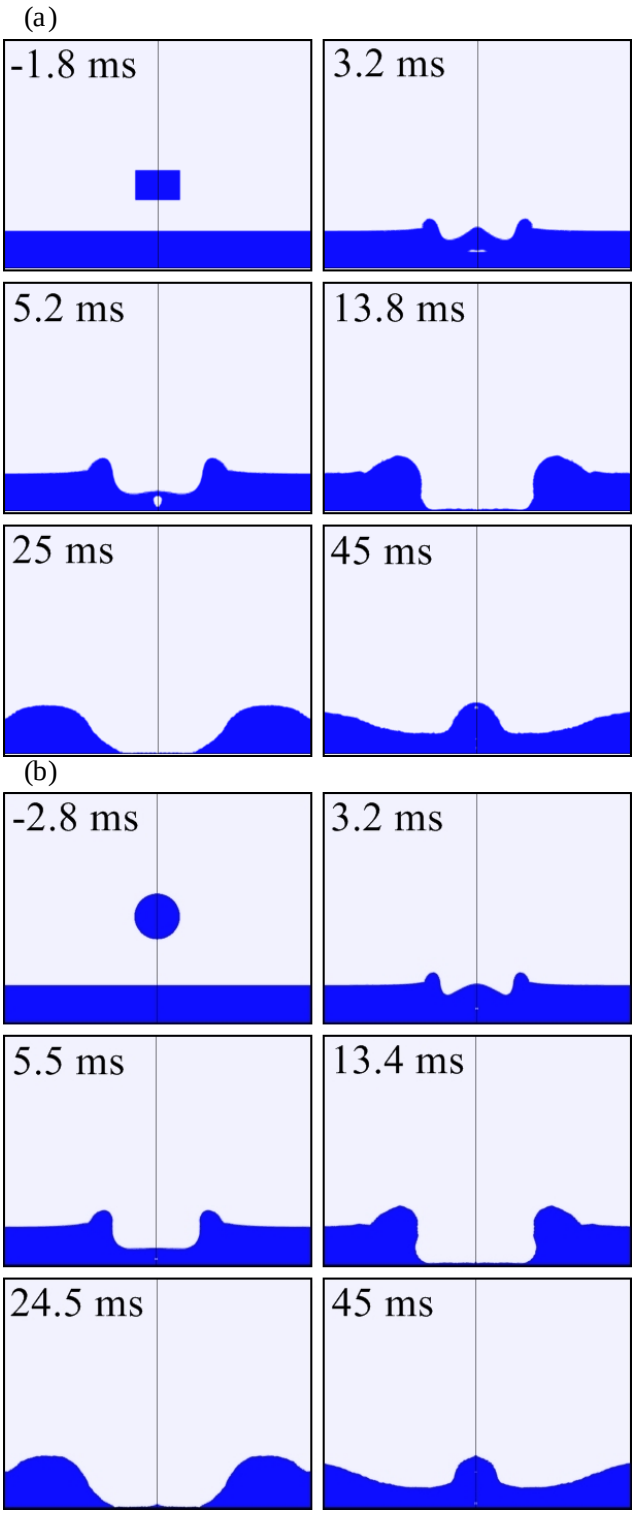

Fig. 22 Single drop impact onto a wet surface in Earth gravity for:
(a) Cylindrical drop with D = 4.48 mm, L = 2.987 mm (equal volume cylinder)
(b) Case 3 spherical drop with D = 4.48 mm

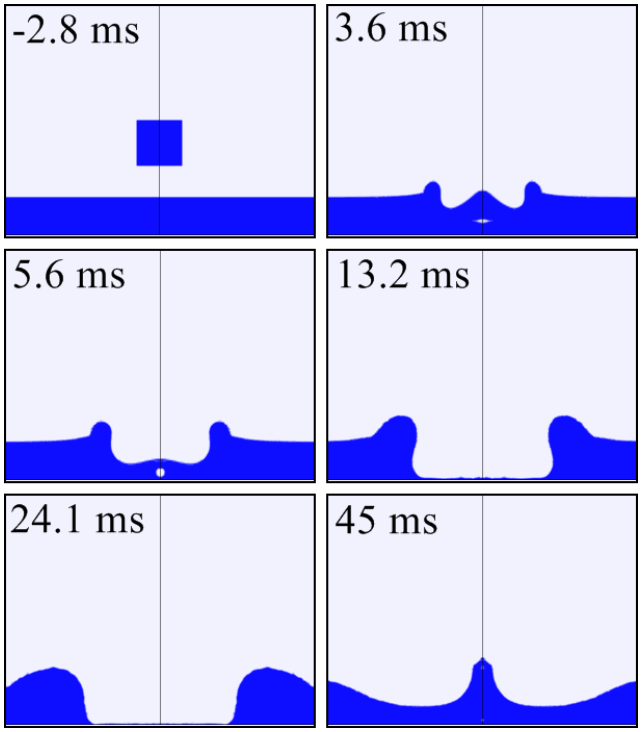

Fig. 23 Equal altitude cylindrical drop impact onto a wet surface in Earth gravity with D = 4.48 mm, L = 4.48 mm (150% volume of the Case 3 spherical drop)

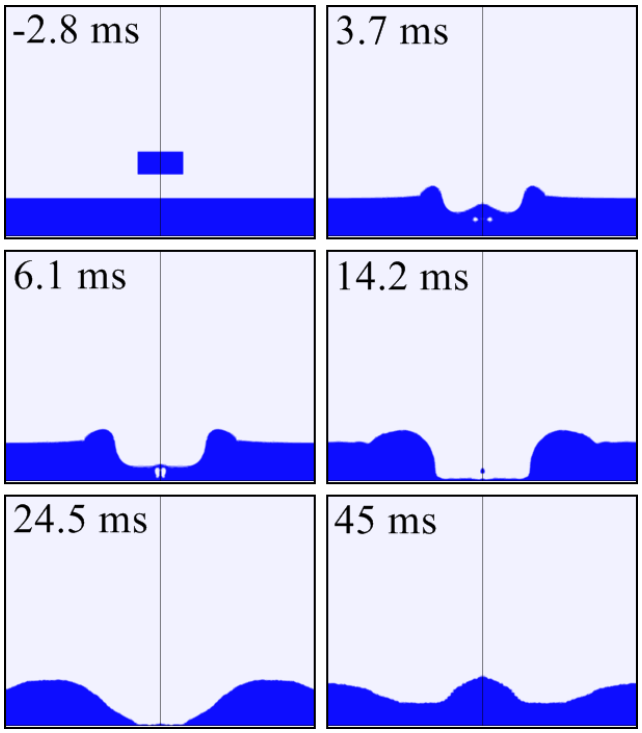

Fig. 24 Half altitude cylindrical drop impact onto a wet surface in Earth gravity with D = 4.48 mm, L = 2.24 mm (75% volume of the Case 3 spherical drop)

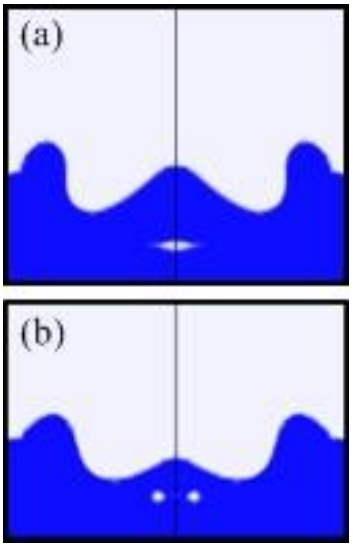

Fig. 25 Comparison of bubble for (a) Equal altitude cylinder at t = 3.6 ms, (b) Half altitude cylinder at t = 3.7 ms

IV. Conclusions

The goal of the present research project is to create a model for spray cooling that is sufficiently accurate to yield reliable predictions, yet sufficiently simple to be a practical design tool. Kreitzer and Kuhlman [2] have formulated a preliminary version of such a model based on a Monte Carlo approach. In order to upgrade this model to the required level of physical realism, more accurate correlation equations for such parameters as maximum crater radius and minimum layer depth must be determined and incorporated. Both experimental and computational methods are being used to obtain these correlations. The simulations presented here are early results from the computational study. Much additional work remains before the needed correlations are finalized.

The commercial CFD code ANSYS 14 Fluent has been used to study the impact of single drops of water onto shallow water layers. The simulations were for 2D-axisymmetric domains with adaptive mesh refinement. The models used in Fluent were the explicit Volume of Fluid method, the Pressure Implicit with Splitting of Operators algorithm, the Piecewise Linear Interface Calculation scheme, and the Continuum Surface Force model.

Simulations of drop impacts were run for gravitational accelerations ranging from extremely large (Solar) to zero. While the general evolution of the craters was similar, the rate at which they evolved increased along with the value of g. The impact of an upward moving drop on a downward facing layer caused a significantly different flow, as it excited a Rayleigh-Taylor instability which caused the liquid to fall off of the ceiling.

Laboratory observations have found that water drops in the 4-mm size range are not true spheres when they impact a liquid layer. To explore the importance of nonspherical drop shapes, three cylindrical drops were simulated, even though there is no known method to produce such shapes in the laboratory. While there were definite differences compared to the impact of a sphere, the overall similarity of the flows produced by these radically different drop shapes implies that the much smaller deviations from sphericity which occur in reality need not be considered in order to obtain realistic simulations.

Acknowledgment

The authors thank their experimentalist collaborators Dr. John M. Kuhlman, Nicholas L. Hillen, and J. Steven Taylor for many stimulating discussions.

References

[1] Silk, E. A., Golliher, E. L., Selvam, R. P., "Spray cooling heat transfer: technology overview and assessment of future challenges for micro-gravity application", *Energy Conversion and Management*, Vol.49, 2008, pp. 453-468.

[2] Kreitzer, P. J., Kuhlman, J. M., "Spray cooling droplet impingement model", Paper AIAA-2010-4500, AIAA 10th AIAA/ASME *Joint Thermophysics and Heat Transfer Conference*, Chicago, IL, June 28-July 1, 2010.

[3] Yarin, A. L., "Drop impact dynamics: splashing, spreading, Receding, Bouncing…", Annual Review of Fluid Mechanics, Vol.38, 2006, pp. 159-192.

[4] Hillen, N. L., Kuhlman, J. M, Dinc, M., Gray, D. D., 2012, "Drop impingement on wet and dry surfaces," Paper AIAA 2012-2960, AIAA 42nd *Fluid Dynamics Conference and Exhibit*, New Orleans, LA, June 25-June 28, 2012.

[5] Ariafar, K., "Performance evaluation of a model thermocompressor using computational fluid dynamics", *International Journal of Mechanics*, Issue 1, Volume 6, 2012, pp. 35-42.

[6] Ghandriz, A. R., Goudarzi, B. M., "Comparison of a pressure correction based solver VoF method in moving floor container", *International Journal of Mechanics*, Issue 1, Volume 3, 2009, pp. 1-8.

[7] Shao, B., Cheng, H., Li, J., Li, Z., Hou, L., Hou, J., Wang, L., "Numerical simulation of complex flow field in quenching furnace with mixture of Nitrogen-spray water eject quenching under normal pressure and high velocity", *International Journal of Mechanics*, Issue 4, Volume 3, 2009, pp. 53-60.

[8] Torfi, S., Nejad, S. M., "Numerical model for vaporization simulation of a single droplet", *International Journal of Mechanics*, Issue 2, Volume 5, 2011, pp. 75-82.

[9] Hirt, C. W., Nichols, B. D., "Volume of Fluid (VOF) method for the dynamics of free boundaries", *Journal of Computational Physics*, Vol.39, 1981, pp. 201-225.

[10] Brackbill, J. U., Kothe, D. B., Zemach, C., "A continuum method for modeling surface tension", *Journal of Computational Physics*, Vol.100, 1992, pp. 335-354.

[11] Issa, R. I., "Solution of implicitly discretized fluid flow equations by operator splitting", *Journal of Computational Physics*, Vol.62, 1986, pp. 40-65.

[12] Rider, W. J., Kothe, D. B., "Reconstructing volume tracking", *Journal of Computational Physics*, Vol.141, 1998, pp. 112-152.

[13] Wang, A.-B., Chen, C.-C., "Splashing impact of a single drop onto very thin liquid films", *Physics of Fluids*, Vol.12, No.9, 2000, pp. 2155-2158.

[14] Asadi, S., Passandideh-Fard, M., "A computational study on droplet impingement onto a thin liquid film", *The Arabian Journal for Science and Engineering*, Vol.34, No.2B, 2009, pp. 505-517.

[15] http://www.spacedaily.com/reports/Astronomers_Plan_Last_Look_at_Asteroid_1999_RQ36_Before_OSIRIS_REx_Launch_999.html, accessed 9/19/2012.

Biography

Murat Dinc was born in Kayseri, Turkey on 10 June, 1985. He received his Bachelor degree from Mechanical Engineering Department at Gazi University, Ankara in Turkey. He received his Master degree from Department of Mechanical Engineering at University of Nevada, Reno. He was a Graduate Research Assistant and worked on the research project sponsored by the Nevada Department of Transportation. His Master thesis was "The Improvements of Snow Plowing Safety and Efficiency: Computational Modeling and Experimental Verification". He has started his PhD as a Graduate Research Assistant in the Department of Civil and Environmental Engineering at West Virginia University in 2011.

Donald D. Gray is Professor and Group Coordinator for Environmental and Hydrotechnical Engineering in the Department of Civil and Environmental Engineering at West Virginia University. He wrote *A First Course in Fluid Mechanics for Civil Engineers* (Water Resources Publications, 2000) and is the author or co-author of more than 200 papers, reports, and conference presentations on fluid mechanics. A native of New Orleans, he holds degrees from Tulane University (B.S.E.(M.E.)) and Purdue University (M.S.E. and Ph.D.).